Journal of Nanobiotechnology

RESEARCH Open Access

ROS-responsive simvastatin nano-prodrug based on tertiary amine-oxide zwitterionic polymer for atherosclerotic therapy

Haiqin Yang[1], Mengcheng Guo[1], Qingran Guan[1], Lixue Zhang[1], Man Liu[1], Haoyu Li[2], Guanyu Qiao[3], Qingbiao Yang[4], Meili Shen[3] and Yapeng Li[1*]

Abstract

Atherosclerosis (AS) is a major cause of cardiovascular disease and is characterized by high levels of reactive oxygen species (ROS) and lipid deposition. This study utilized ROS-responsive oxalate bonds to conjugate simvastatin (SV) and tertiary amine-oxide zwitterionic polymer (OPDH), resulting in the design of a ROS-responsive simvastatin nano-prodrug (OPDH-SV). In vitro experiments have proved that OPDH-SV has excellent stability and low toxicity, can effectively reduce intracellular ROS and lipid levels, and inhibit foam cells formation. In addition, OPDH-SV is able to achieve cell-to-cell transmission through the cell's "endocytosis-efflux" mechanism and target mitochondria. In vivo experiments further confirmed the long-term circulation, targeted enrichment, and reduction of ROS and lipid levels of OPDH-SV in vivo. In summary, OPDH-SV has good biosafety and excellent in vivo therapeutic effect, and is expected to become a new type of anti-atherosclerotic nano-prodrug.

*Correspondence:
Yapeng Li
liyapeng@jlu.edu.cn
[1]Key Laboratory of Special Engineering Plastics Ministry of Education, College of Chemistry, Jilin University, Changchun, Jilin 130012, China
[2]Department of Spine Surgery, The First Hospital of Jilin University, 1 Xinmin Street, Changchun, Jilin 130021, China
[3]Department of Radiation Oncology, China-Japan Union Hospital of Jilin University, Changchun, Jilin 130033, China
[4]College of Chemistry, Jilin University, Changchun, Jilin 130021, China

Graphical Abstract

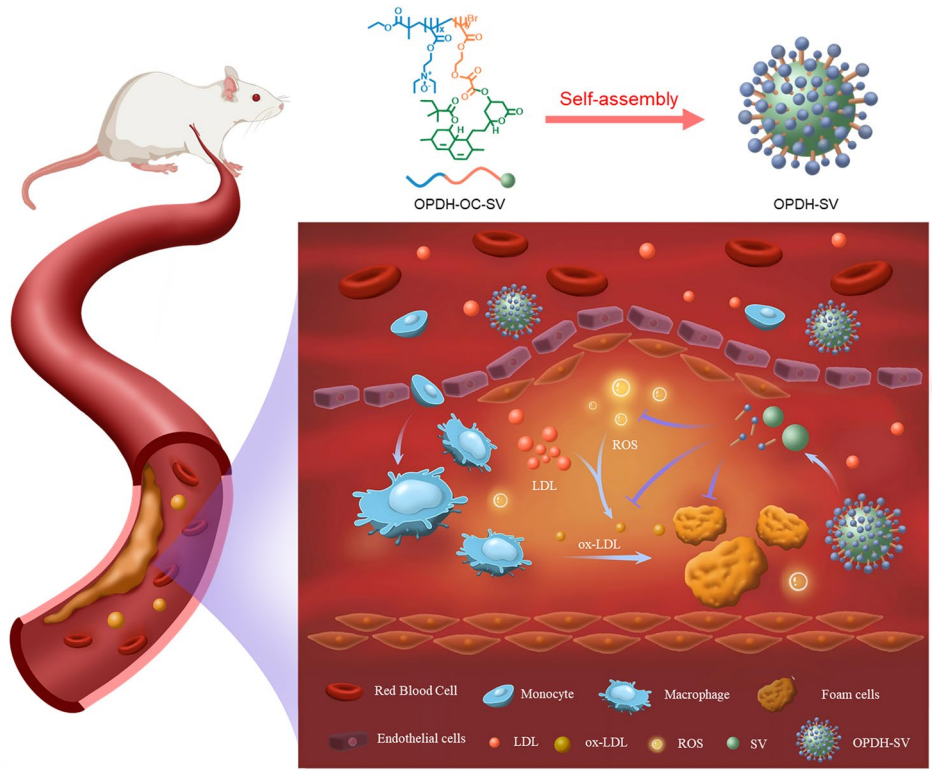

Schematic diagram of OPDH-SV for the treatment of atherosclerotic plaques

Keywords Atherosclerosis, Nano-Prodrug, Active transcytosis, Long-acting circulation, ROS response

Introduction

AS is a chronic inflammatory cardiovascular disease characterized by the deposition of lipids, immune cells, and fibrous elements within the artery walls to form plaques, leading to narrowing and hardening of blood vessels and producing high concentrations of ROS [1]. The "China Cardiovascular Health and Disease Report 2023" reveals that the number of cardiovascular disease patients caused by AS has reached 330 million, with a 57.39% increase in mortality rate compared to last year, imposing an economic burden of up to 165.2 billion on the country [2, 3]. Reducing the incidence of cardiovascular diseases has become an urgent issue to be addressed. At present, the clinical treatment of AS is mainly based on drug therapy with statins being the first-line clinical drugs. They can not only regulate blood lipids and reduce cholesterol and triacylglycerol levels by inhibiting HMG-CoA reductase [4, 5], but also have antioxidant, anti-inflammatory, improve endothelial function and antithrombotic effects. These multifaceted actions help to delay plaque progression and prevent the occurrence of cardiovascular diseases [6, 7]. However, there are some challenges in the clinical application of statins, such as large toxic side effects (muscle damage, hepatotoxicity, type 2 diabetes), which limit the drug dose [8–10]. Poor water solubility, which affects drug absorption and distribution. Rapid renal clearance, which results in a short duration of action. These factors limit their efficacy and systemic bioavailability [11–13].

The emerging interdisciplinary field of nanomedicine offers an innovative approach for the targeted delivery of small molecule drugs against AS [12, 14]. Nano-prodrug is an inactive drug conjugate that can be converted into an active pharmaceutical ingredient (API) in vivo [15], which has the characteristics of reducing drug toxicity, increasing drug lesion enrichment and improving pharmacokinetics, and has become a frontier research hotspot [16, 17]. The design of ROS-sensitive nano-prodrugs and the use of overexpressed ROS in the AS environment as the trigger for the release of active drugs. This approach enables efficient enrichment of active drugs in lesion sites without drug activity in non-lesion sites,

thereby reducing drug toxicity and side effects [18–21]. In addition, zwitterionic polymers, as nano-prodrug carrier materials, have become a research hotspot in recent years due to their excellent hydrophilicity, anti-protein adsorption properties and long-term circulation in vivo [22–24]. Shen's team found that the zwitterionic polymer OPDEA, which contains a tertiary amine nitrogen oxygen structure (N^+-O^--), can be used as a zwitterionic nano-drug delivery platform [25]. The N^+-O^- structure can reversibly adhere to erythrocytes to achieve long-term blood circulation. Additionally, it triggers transcytosis of endothelial cells, facilitating efficient intracellular delivery through transcellular transport and enhancing the enrichment of drugs at lesion sites [26–28]. N^+-O^-- novel zwitterionic polymers have great potential in the design of nanodrug carriers, which can help overcome the shortcomings of traditional zwitterionic nano-prodrugs that cannot trigger cell transcytosis [29], and provide a new strategy for the treatment of atherosclerosis and other diseases.

In this study, a ROS-responsive simvastatin nano-prodrug with active transcytosis (OPDH-SV) was designed for atherosclerotic therapy. The N^+-O^-- zwitterionic polymer Poly [2-(N-oxide-N, N-diethylamino) ethyl methacrylate-hydroxyethyl methacrylate] (OPDH) was synthesized via aggregation using ATRP technology. Subsequently, simvastatin (SV) and OPDH were conjugated through a ROS-responsive oxalate ester bond to form the self-assembled simvastatin nano-prodrug OPDH-SV. As shown in Scheme 1, the drug delivery system can not only achieve high enrichment at the plaque site through active transcytosis characteristics, but also maintain drug inertia in healthy sites, and specifically release the active drug ingredient simvastatin at the plaque site to exert antioxidant and lipid-lowering effects, which designs a "double insurance" to reduce drug toxicity and side effects, and greatly improves the antithrombotic efficacy, providing new ideas for atherosclerotic treatment.

Results and discussion

Preparation and characterization of OPDH polymer prodrug modification OPDH-SV

First, PDH was synthesized by ATRP between DEA and HEMA, and then PDH was oxidized by H_2O_2 to form OPDH amphoteric ion. The oxalate ester linkage and OPDH were covalently coupled to the simvastatin hydroxy lactone ring to obtain simvastatin prodrug OPDH-OC-SV. The synthesis pathway of OPDH-OC-SV was illustrated in Fig. S1. PDH, OPDH, and OPDH-OC-SV were successfully prepared by ^{1}H NMR spectroscopy and FT-IR spectroscopy. In ^{1}H NMR spectra, the position peak of methylene (e) next to the N-O bond of OPDH changed from 2.57 ppm to 3.30 ppm, and the position peak of methyl group (f) near to N-O bond changed from 1.04 ppm to 1.26 ppm (Fig. S2a and S2b) and the SV characteristic peaks of OPDH-OC-SV were 5.37 ppm, 5.52 ppm and 5.82 ppm (Fig. S2c and S2d). According to the FT-IR spectra, OPDH showed the characteristic structure N-O absorption peak in zwitterion at 2810 cm^{-1} (Fig. S3). All of the above results confirmed the successful synthesis of PDH, OPDH, OPDH-OC-SV.

Amphiphilic OPDH-OC-SV was used to form ROS-responsive simvastatin nano-prodrug OPDH-SV with active transcytosis through self-assembly. As shown in Fig. S4, the UV-Vis absorption spectrum of SV changes at 238 nm after preparation of OPDH-OC-SV and OPDH-SV. Further indicates the successful synthesis of OPDH-OC-SV and OPDH-SV. The size, Zeta potential, encapsulation efficiency, and drug loading of the nano-prodrug were investigated by changing the molar ratio of the hydrophilic and phobic ends (n_{DEA}:n_{HEMA}) (Table S1 and Fig. 1a). The results showed that the optimal drug loading (28.30 ± 1.31%) was obtained under the condition of the molar ratio of OPDH-SV was 3:1, and the particle size was small (118.96 ± 3.36 nm), and the Zeta potential was − 4.61 ± 0.87 mV, so the OPDH-SV with a molar ratio of 3:1 was used in subsequent experiments. As shown in Fig. 1b, the OPDH-SV nano-prodrug has a uniform spherical structure, and the measured particle size is smaller than that determined by DLS due to the hydrophilic shell shrinkage of the nano-prodrug during TEM preparation. The long-term stability of OPDH-SV in PBS solution containing 10% fetal bovine serum (FBS) was further investigated by DLS, and it was found that the particle size and Zeta potential of OPDH-SV did not change significantly within 14 days, indicating that the stability of OPDH-SV was satisfactory when mimicking the blood environment (Fig. 1c and d). In addition, OPDH-SV exhibits charge reversal characteristics at different pH values: 41.5 mV at pH = 5 and − 5.5 mV at near-neutral pH = 7 (Fig. 1e). The change in charge from positive to negative is due to the state variation of N-oxide groups on the OPDH surface at different pH values. They are non-ionic at neutral pH, but undergo protonation and exhibit cationic characteristics at acidic pH [29]. The charge reversal characteristic enables OPDH-SV to enhance endocytosis, prolong blood circulation time, and improve the enrichment degree of drugs in the lesion site under the condition of lesion microenvironment (pH = 5.8). This characteristic makes OPDH-SV a potential application advantage in different physiological environments.

ROS-responsive drug release

In the course of atherosclerotic lesions, the inflammatory response within the plaque causes the local microenvironment to become acidic, accompanied by an excess of ROS. This specific pathological microenvironment

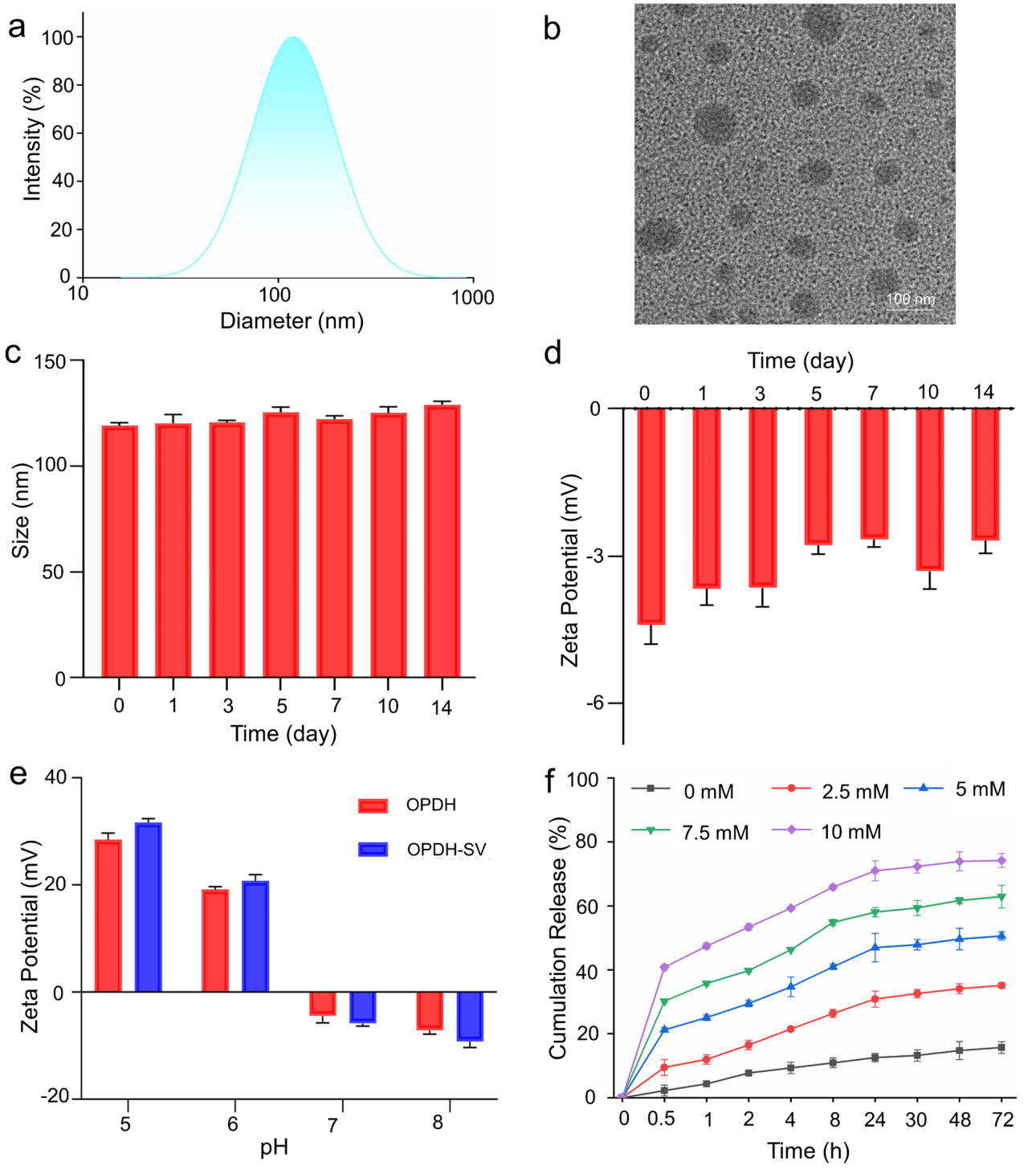

Fig. 1 **(a)** Particle size map of OPDH-SV; **(b)** TEM plot of OPDH-SV, scale bar = 100 nm; **(c)** Particle size and **(d)** Zeta potential stability of OPDH-SV in PBS solution of 10% fetal bovine serum (FBS) within 14 days; **(e)** Zeta potential of OPDH and OPDH-SV at different pH conditions; **(f)** Cumulative release of simvastatin at different H_2O_2 concentrations. Data are presented as mean ± SD ($n = 3$)

provides an ideal trigger for the design of responsive nanodrug carriers. The active form of simvastatin is its β-hydroxy acid form, which is formed by hydrolysis of the β-hydroxy lactone ring in its prodrug form in vivo [15]. However, hydroxyl substitution on the lactone ring may hinder the hydrolysis process, affecting the activity of the drug [30]. To solve this problem, we used a ROS-sensitive chemical bond, the oxalate ester bond, to link the

hydroxyl group on simvastatin to form OPDH-OC-SV. In our study, the OPDH-SV nano-prodrug was able to specifically cleave and release simvastatin in environments with high ROS concentrations (Fig. S5), such as atherosclerotic plaques. By high-performance liquid chromatography (HPLC) analysis, we measured the amount of simvastatin released by OPDH-SV over time at different concentrations of hydrogen peroxide. The results showed that the peak location of the released drug was consistent with that of simvastatin, and the release of simvastatin increased with the increase of hydrogen peroxide concentration and duration of action, which was reflected in the increase in the characteristic peak area of simvastatin in the HPLC profile (Fig. S6a and S6b). In addition, we established the SV curvature by UV spectrophotometry (Fig. S6c) and analyzed the drug release curves of simvastatin in OPDH-SV at different H_2O_2 concentrations. In the absence of H_2O_2, simvastatin in OPDH-SV is released at an extremely slow rate, reaching only 15.8% within 72 h. However, when co-incubated with 1 mM H_2O_2 for 72 h, simvastatin release increased to 35.2%. More significantly, simvastatin release was significantly increased to 74.2% after 72 h of incubation with 10 mM H_2O_2 (Fig. 1f). These results suggest that with the increase of H_2O_2 concentration, the nano-prodrug structure of OPDH-SV suffers more severe damage, thereby accelerating the release of simvastatin. There was a significant concentration dependence between the release rate of simvastatin and the concentration of H_2O_2. In summary, our results confirm that OPDH-SV, as a ROS-responsive prodrug carrier, can effectively release simvastatin in the presence of ROS, providing a potential targeted drug delivery strategy for the treatment of atherosclerosis.

Cytotoxicity

Cytotoxicity is an important indicator to assess the safety of a drug. Zwitterionic polymers are neutral, exceptional superhydrophilicity, and have low protein-cell interactions, resulting in slower cellular internalization and lower cytotoxicity [31]. As shown in Fig. 2a, OPDH-SV exhibited low cytotoxicity after 24 h incubation in HUVEC and RAW 264.7 cells, with cell viability remaining at approximately 80% in the OPDH and OPDH-SV treated groups at concentrations up to 64 μg/mL, compared to 55% after treatment with the same concentration of free SV. The results showed that nano-prodrug could effectively reduce cytotoxicity and improve biocompatibility.

Macrophage cells uptake

Macrophages play a key role in the development of atherosclerosis [32], and their uptake of nanodrugs is one of the necessary conditions to affect the therapeutic effect [33]. We used inverted fluorescence microscopy and flow cytometry to investigate the uptake of nano-pharmaceuticals by macrophages. The red fluorescence of Nile Red (NR)-labelled OPDH-SV (OPDH-SN) was evident in macrophage cells (RAW 264.7) after incubation with the cells for different times, and gradually increased with the longer the incubation time. Fairly high fluorescence intensities were observed even after 0.5 h of incubation, suggesting that RAW 264.7 cells were able to endocytose OPDH-SN rapidly and in a time-dependent manner (Fig. 2b). In contrast, free NR was poorly water-soluble and RAW 264.7 cells had lower uptake (Fig. S7a). OPDH-SN was confirmed by flow cytometry and fluorescence intensity quantification to be more easily absorbed by cells than free NR (Fig. 2c and d, Fig. S7b and S7c). In addition, we investigated the uptake of RAW 264.7 cells by different concentrations of OPDH-SN. Both inverted fluorescence microscopy and flow cytometry analysis showed that the uptake of OPDH-SN by RAW 264.7 cells was concentration-dependent (Fig. 2e-g).

In vitro study of the endocytic mechanism of OPDH-SN by HUVEC cells

Different endocytic inhibitors were used to study the endocytic mechanism of OPDH-SN in HUVEC cells. β-CD is a caveolin-mediated endocytosis inhibitor and CCD is a macropinocytosis inhibitor, both of which significantly reduce OPDH-SN uptake by HUVEC cells, while Sucrose is a clathrin-dependent endocytosis inhibitor with no significant effect on cellular uptake of OPDH-SN (Fig. S8b and S8d). These results demonstrate that OPDH-SN entry into HUVEC cells is achieved through macropinocytosis and caveolin-mediated endocytosis pathways. In contrast, the endocytosis of NR was inhibited only by β-CD, while the other two inhibitors did not exhibit significant inhibitory effects, suggesting that NR is dependent on the caveolin-mediated endocytic pathway internalized by HUVEC cells (Fig. S8a and S8c).

Ability to target mitochondria

Since AS is associated with mitochondrial dysfunction, targeting mitochondria can reduce inflammation and oxidative stress, thereby slowing the progression of atherosclerosis [34]. Mitochondrial localization was performed using Mito-Tracker Green to evaluate the mitochondrial targeting ability of nano-prodrugs. As shown in Fig. 3a, the yellow fluorescence of OPDH-SN was strong after entering RAW 264.7 cells, indicating that there were more overlapping regions of red fluorescence and green fluorescence, confirming that OPDH-SN can target mitochondria in RAW 264.7 cells. To further analyze the mitochondrial localization of OPDH-SN in cells, we performed fluorescence scans on two randomly plotted linear paths in RAW 264.7 cells, as shown in Fig. 3b-d, the NR signal was highly consistent with the

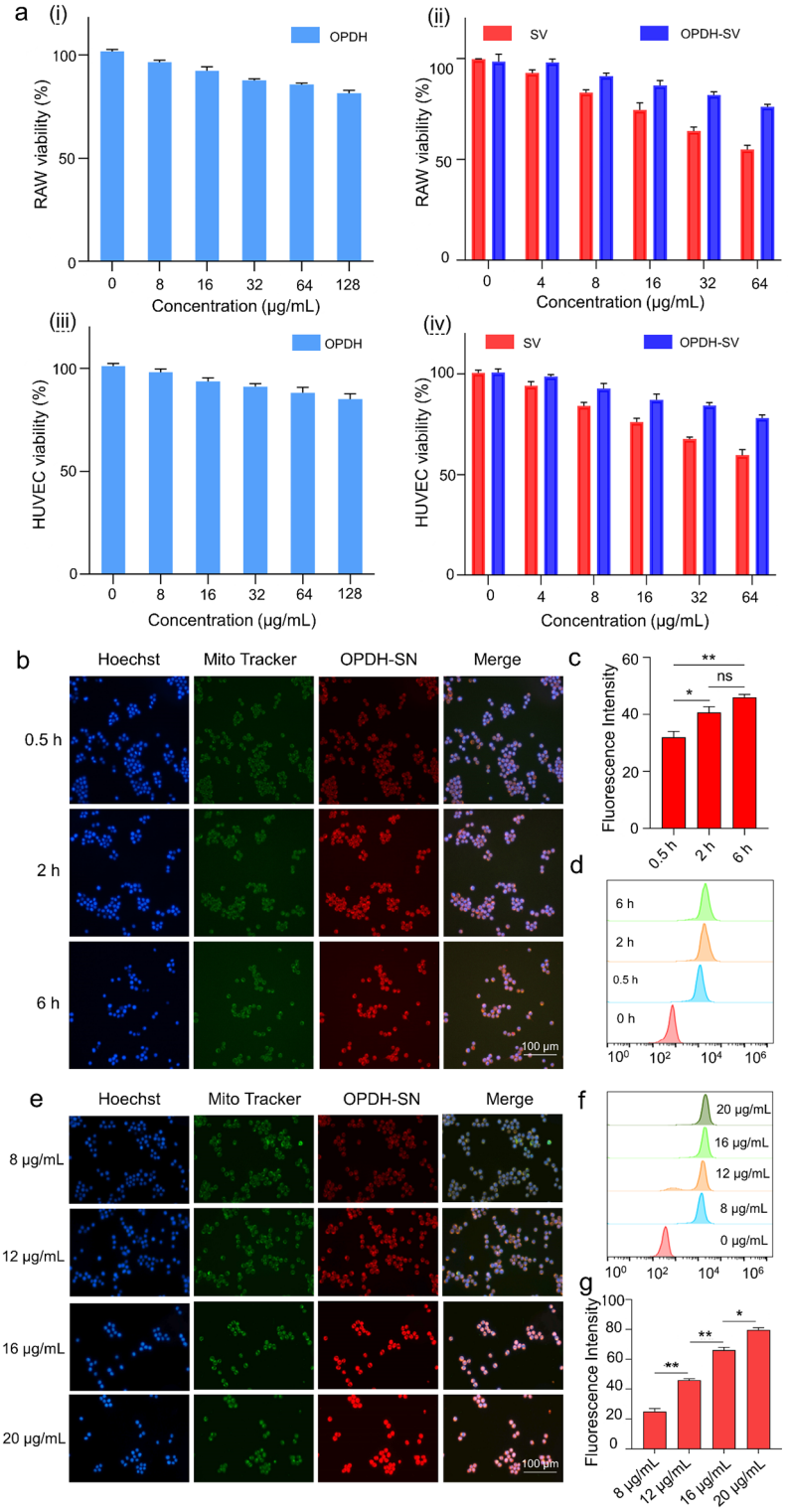

Fig. 2 **(a)** Cytotoxicity of OPDH, SV and OPDH-SV, (i) Cell viability of RAW 264.7 after 24 h of OPDH treatment, (ii) Cell viability of RAW 264.7 after 24 h of SV and OPDH-SV treatment, (iii) Cell viability of HUVEC after 24 h of OPDH treatment; (iv) Cell viability of HUVEC after 24 h of SV and OPDH-SV treatment; The inverted fluorescence microscope **(b)** and flow cytometry **(c)** were used to observe the cellular uptake of OPDH-SN by RAW 264.7 cells after different incubation times, and the fluorescence intensity of uptake at different time points was quantified **(d)**, scale bar = 100 μm; Cell uptake at different concentrations of OPDH-SN after incubation with RAW 264.7 cells for the same time was observed using inverted fluorescence microscopy **(e)** and flow cytometry **(f)**, fluorescence intensities at different concentrations were quantified **(g)**, scale bar = 100 μm. The data are represented as mean ± SD ($n = 3$), *$p < 0.05$, **$p < 0.01$, ***$p < 0.001$, ns, no significance

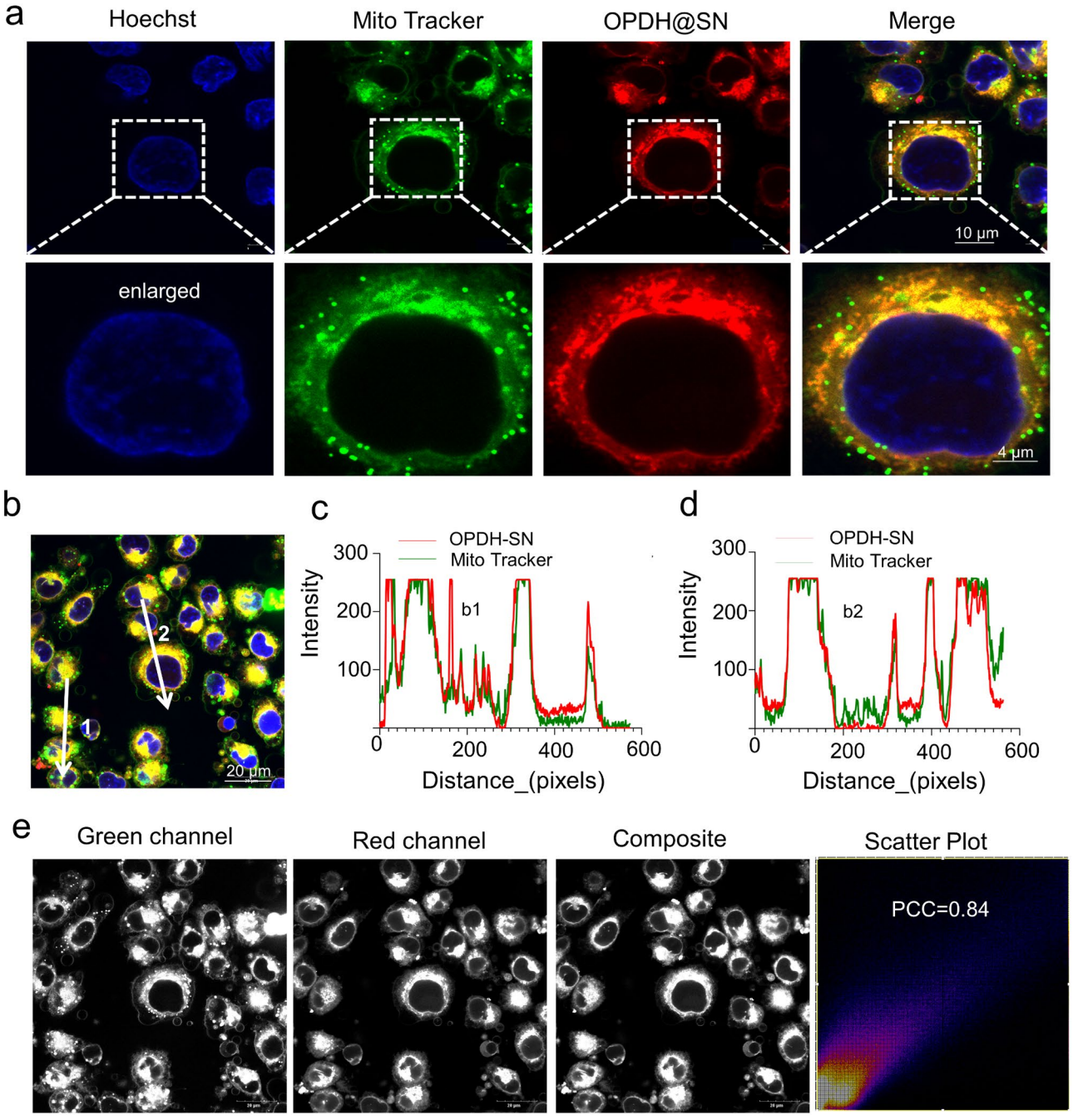

Fig. 3 **(a)** CLSM was used to observe the colocalization of OPDH-SN (red) and mitochondria (green) after incubation with RAW 264.7 cells for 4 h, blue indicates nucleus, yellow is the overlap of red and green fluorescence, scale bar = 10 μm, 4 μm; **(b)** CLSM was used to observe the distribution of OPDH-SN in RAW 264.7 cells, scale bar = 20 μm; **(c)** Fluorescence analysis of b1; **(d)** Fluorescence analysis of b2; **(e)** PCC analysis results obtained by Image J software after analysis and processing of CLSM images

peak of the Mito-Tracker Green signal on the scan line, which strongly supported the mitochondrial targeting of OPDH-SN nano-prodrugs. Pearson correlation coefficient (PCC) analysis was also performed on confocal (CLSM) images. The purpose of this analysis was to detect the correlation of the value range within $-1 \sim 1$, where 0 indicates no significant correlation, and -1 and 1 represent strong negative and positive correlations, respectively. A good overlap of the two channels should appear as a linear distribution of scatterplots, and the PCC value should be close to 1 [35]. As shown in Fig. 3e, the PCC coefficient was 0.84, a positive value indicating a positive correlation between the green and red channels,

further indicating that OPDH-SN was distributed within the mitochondria of RAW 264.7 cells.

ROS clearance performance

ROS has important biological functions in living organisms, and oxidative stress caused by excess reactive oxygen species has become one of the key mechanisms in the development of atherosclerosis. Excessive accumulation of ROS in atherosclerosis increases the production of oxidized low-density lipoprotein (ox-LDL), which stimulates plaque formation [36, 37]. Therefore, we used inverted fluorescence microscopy to study the regulation of ROS levels in inflammatory cells by OPDH-SV, and the intensity of the green fluorescence signal was derived from the DCFH-DA fluorescent probe to indicate ROS levels. As shown in Fig. 4a and b, the production of ROS in RAW 264.7 cells induced by LPS was significantly increased, but the fluorescence intensity decreased significantly after co-incubation with the same concentration of free SV and OPDH-SV with pretreated RAW 264.7 cells for 4 h. In particular, green fluorescence was almost not observed in OPDH-SV treated cells, and in the absence of SV loading, OPDH had little inhibitory effect on ROS production. This suggests that the antioxidant properties of SV are a key factor. Further quantitative analysis by flow cytometry confirmed the effective clearance of ROS by OPDH-SV (Fig. 4c).

Transcellular transmission of OPDH-SN

We validated the transcytosis of OPDH based on the "endocytosis-efflux" mechanism through cross-cell delivery experiments. As shown in Fig. 4d and S9a, after co-incubation with different concentrations of OPDH-SN with HUVEC and RAW 264.7 cells for 5 h, significant red fluorescence was observed in the $1^{\#}$ dish by inverted fluorescence microscopy, indicating that a large amount of OPDH-SN was taken up by the cells. Subsequently, the medium in the $1^{\#}$ dish was replaced with fresh medium and continued to incubate for 12 h, and the results showed that the intracellular fluorescence signal in the $1^{\#}$ dish was significantly weakened, indicating that part of the OPDH-SN was excreted by the cells. After then incubating the medium collected in the $1^{\#}$ dish with the cells in the $2^{\#}$ dish for 12 h, a strong fluorescent signal appeared in the cells in the $2^{\#}$ dish, which proved that the cells in the $1^{\#}$ dish released OPDH-SN into the medium through efflux and thus were taken up by the cells in the $2^{\#}$ dish. Similarly, the red fluorescent signal of OPDH-SN was also observed in $3^{\#}$ cells, indicating that $2^{\#}$ cells can be taken up by cells in $3^{\#}$ dishes by transcytosis after they are effluxed into the medium by transcytosis. Moreover, with an increase in the concentration of OPDH-SN, there is enhanced cellular internalization and excretion, resulting in a stronger fluorescence intensity (Fig. 4e and f, Fig. S9b and S9c). The results showed that OPDH-SN could continuously carry out intracellular endocytosis and extracellular efflux, and realize active transcytosis and transcellular transmission between cells. This intercellular transmission enables drugs to efficiently accumulate at the AS lesion site, enhancing the therapeutic effect.

Anti-atherosclerotic formation

ox-LDL is converted into foam cells by macrophage excessive uptake, and foam cell formation is a key pathological feature in areas of atherosclerotic lesions [38]. As shown in Fig. 4g, compared to the control group without ox-LDL, the ox-LDL group produced a large number of foam cells, and the OPDH group without SV loading had no effect on foam cell formation, whilst free SV and OPDH-SV significantly reduced foam cell formation. The results showed that OPDH-SV significantly inhibited the uptake of ox-LDL and the formation of foam cells by RAW 264.7 cells. We further investigated the inhibitory effect of RAW 264.7 on foam cell formation after OPDH-SV stimulation. As shown in Fig. S10, the number of foam cells formed by RAW 264.7 after SV and OPDH-SV stimulation was significantly lower than that in the ox-LDL group, and the number of foam cells in the OPDH-SV group was lower than that in the SV group. In summary, OPDH-SV can significantly inhibit the formation of foam cells and has great potential in anti-atherosclerotic therapy.

Pharmacokinetics of OPDH-SV

Pharmacokinetics is a judging criterion to reflect the circulation time of nanodrugs in vivo, which can be used to confirm whether OPDH-SV has long-acting circulating properties in vivo. After rats were injected with SV or OPDH-SV via the tail vein, blood samples were collected at regular intervals and SV concentrations were quantified using HPLC. As shown in Fig. 5a and Table S2, free SV was rapidly cleared from the blood after tail vein administration with a half-life of 1.59 h and an area under the curve ($AUC_{0-\infty}$) of 21.22 μg $mL^{-1}h^{-1}$, compared to a significantly longer blood circulation time of OPDH-SV with a half-life of 21.06 h and an area under the curve ($AUC_{0-\infty}$) of 408.19 μg $mL^{-1}h^{-1}$. The superior pharmacokinetics of OPDH-SV may be attributed to the properties of zwitterionic OPDH, which does not easily bind to proteins, whilst at the same time achieving a "free-rider" effect through the binding of red blood cell surfaces [39, 40].

Targeted effects and in vivo therapy of OPDH-SV

We established an atherosclerosis model by feeding $ApoE^{-/-}$ mice with a high-fat diet, and studied the accumulation of OPDH-SV at the site of atherosclerotic lesions. As shown in the ex vivo imaging results in

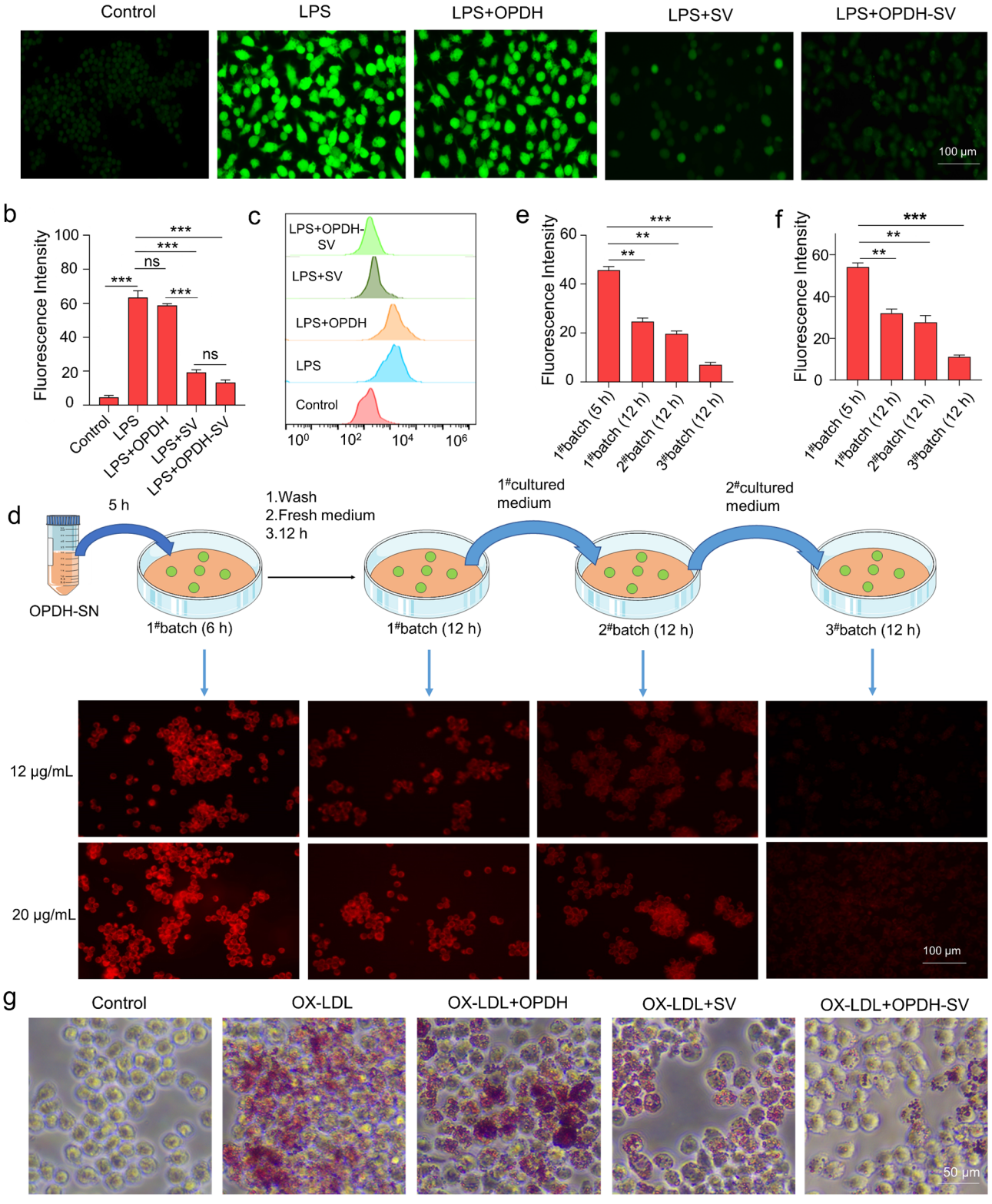

Fig. 4 **(a)** The production of ROS in RAW 264.7 cells stimulated by different drugs after DCFH-DA staining was observed by inverted fluorescence microscopy, scale bar = 100 μm; **(b)** Intracellular ROS fluorescence quantification; **(c)** Flow cytometry spectra of ROS in RAW 264.7 cells stimulated by different drugs; **(d)** Flowchart and inverted fluorescence microscopy of cross-cell transmission of different concentrations of OPDH-SN in RAW 264.7 cells, scale bar = 100 μm; Quantitative analysis of the fluorescence intensity of OPDH-SN at 12 μg/mL **(e)** and 20 μg/mL **(f)** in RAW264.7 cells. **(g)** Microscopic view of ox-LDL-induced foam cell formation in Oil Red O-stained RAW 264.7 cells, scale bar = 50 μm. Data are expressed as mean ± SD ($n = 3$), $^{**}p < 0.01$, $^{***}p < 0.001$, ns, meaningless

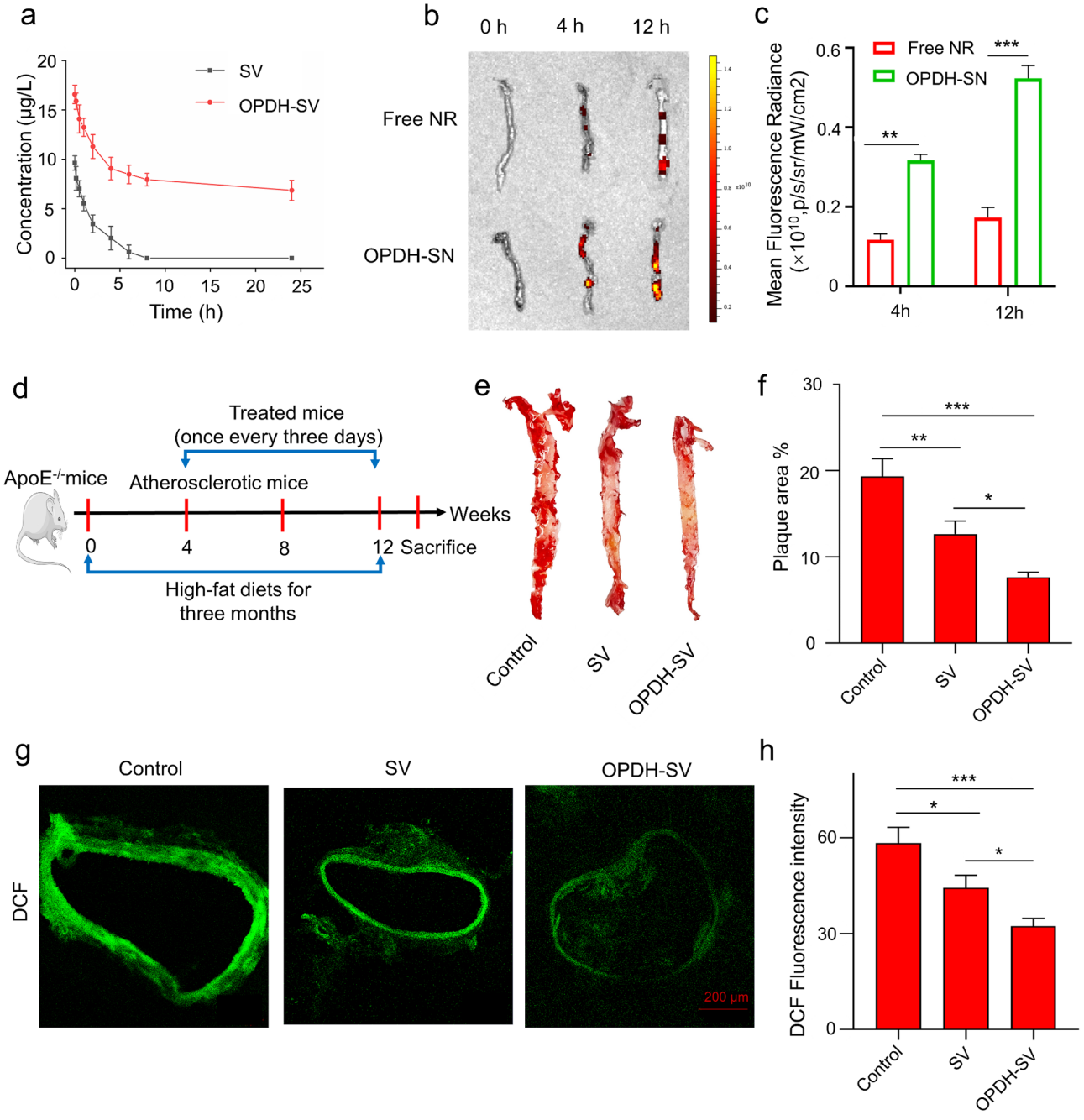

Fig. 5 **(a)** Pharmacokinetic profiles of SV and OPDH-SV at a dose of 15 mg/kg; In vitro images **(b)** and corresponding fluorescence intensities **(c)** of small animals at the site of atherosclerotic lesions after 4 h and 12 h of free NR and OPDH-SN injection; **(d)** Atherosclerosis model establishment and in vivo treatment time chart; Representative images of aortic arch stained with oil red O (ORO) staining in mice after different drug treatments **(e)** and quantitative analysis of ORO in corresponding plaques **(f)**; CLSM image **(g)** and corresponding DCF fluorescence quantitative analysis plot **(h)** of aortic arch section of atherosclerotic mice, scale bar = 200 μm. Data are expressed as mean ± SD ($n = 3$), *$p < 0.05$, **$p < 0.01$, and ***$p < 0.001$

Fig. 5b, the target enrichment efficiency of OPDH-SN nano-prodrug in atherosclerotic lesions was better than that of free NR, and the fluorescence signal was more significant after 12 h of injection than at 4 h. Fluorescence quantification further confirmed that the accumulation of OPDH-SN in the aortic arch was superior to that of free NR (Fig. 5c). The significant plaque accumulation of OPDH-SN may be the result of the combined effect of its active transcytosis and long-acting circulation in vivo. We also observed the accumulation of OPDH-SN and free NR in the heart, liver, spleen, lungs, and kidneys (Fig. S11) and found that both had the highest accumulation in the liver, but at the same time, the enrichment in the liver in the OPDH-SN group was lower than that in the NR

group, which in reverse confirmed that the enrichment of OPDH-SN in the aortic arch was higher than that in NR. This excellent targeting efficiency will significantly improve the therapeutic efficacy of atherosclerosis. We then assessed the degree of penetration of FITC-labelled nano-prodrug (OPDH-SV-FITC) in aortic arch plaques and specifically labelled vascular endothelial cells using the CD31 antibody (red). As shown in Fig. S12, the fluorescence intensity of OPDH-SV-FITC (green) is higher than that of free FITC. Indicates that OPDH-SV-FITC can penetrate deep into AS plaques. Quantitative analysis showed that the penetration depth of OPDH-SV-FITC in atherosclerotic plaques was 1.73 times higher than that of free FITC. In summary, the above results fully indicate that OPDH-SV can penetrate deeply at the site of AS lesions.

In the fourth week, drug treatment was administered to $ApoE^{-/-}$ mice with atherosclerosis via tail vein injection, as shown in Fig. 5d. At the end of the treatment cycle, Dissect the aorta of the mouse and perform a longitudinal incision to expose the endothelial lining of the blood vessel, followed by ORO staining, and the percentage of plaque area in the blood vessels is quantified (Fig. 5e and f). The degree of atherosclerosis was reduced in the SV treatment group compared to the saline group, however, due to the high enrichment of OPDH-SV at the thrombus site, the OPDH-SV group showed a more significant atherosclerotic treatment effect, with a nearly 1-fold reduction in plaque area. To further assess the ability of SV to consume ROS, aortic arch sections were stained with DCFH-DA. Since DCFH-DA can be oxidized to DCF by ROS, and the fluorescence intensity of DCF is positively correlated with ROS content, the level of ROS in the aortic arch was qualitatively and quantitatively detected by the detection of DCF fluorescence. The stronger the green fluorescence, the higher the level of ROS. As shown in Fig. 5g and h, the OPDH-SV group had the lowest ROS level, and there was a significant difference compared with the SV group, indicating that the OPDH-SV group had the strongest antioxidant effect. These experimental results are consistent with the results of ROS clearance and inhibition of foam cell formation in cell experiments, which further confirm the excellent performance of OPDH-SV in reducing oxidative stress and lipid lowering in atherosclerotic plaques.

To further investigate the therapeutic effect of OPDH-SV nano-prodrug on atherosclerosis, aortic arch sections were stained using immunomics to assess plaque collagen, matrix metalloproteinase 9 (MMP-9), α-smooth muscle actin (α-SMA) levels, and smooth muscle cell (VSMC) sequencing (Fig. 6). The results of H&E staining showed that in the saline group, the aortic wall was thickened, the VSMC arrangement was disordered, and the original structure was lost, whilst the intima was smooth and the vascular structure was restored after SV and OPDH-SV treatment. During the development of atherosclerosis, VSMCs proliferate in early plaques and collagen production increases, resulting in an enlargement of the plaque area and further narrowing of the lumen of the blood vessels [34]. Masson three-colour staining showed that there was a large amount of collagen (blue) penetration in the plaques of mice in the saline group, whilst the collagen content in the plaques of the other treatment groups gradually decreased. Immunostaining with α-SMA antibody showed that the number of VSMC (dark brown) in the plaques of OPDH-SV-treated mice was significantly reduced, indicating that OPDH-SV could inhibit the luminal stenosis caused by VSMC proliferation. In addition, staining with MMP-9 antibody, OPDH-SV treatment significantly reduced the expression level of MMP-9 (dark blue) compared to the control group, indicating increased plaque stability. In summary, OPDH-SV has a positive therapeutic effect on atherosclerosis in $ApoE^{-/-}$ mice, which can improve vascular structure, thereby effectively inhibiting the continuous expansion of plaque.

In vivo safety evaluation of OPDH-SV

While evaluating the targeting and therapeutic effects of OPDH-SV, the potential toxicity and side effects of OPDH-SV were evaluated in vivo. During the treatment period, there was no significant difference in body weight between the OPDH-SV treated group and the other groups (Fig. S13a), which preliminarily indicates the biosafety of OPDH-SV application. After the treatment, blood and organs were collected and blood lipids, liver and kidney function, and the degree of necrosis of organ tissues were measured. As shown in Fig. S13b-d, the total cholesterol (TC) and low-density lipoprotein (LDL) levels of the SV treatment group were reduced, and the OPDH-SV group showed lower TC and LDL levels, whilst there was no significant difference in the levels of high-density lipoprotein (HDL) among all groups. These results suggest that OPDH-SV retains the lipid-lowering function of SV, which helps to reduce lipid deposition in AS and inhibit plaque development. The results of biochemical analysis showed that compared with the control group, there was no significant change in the liver and kidney function related indices in the OPDH-SV group, indicating that OPDH-SV did not damage the liver and kidney function of mice (Fig. SS14). In addition, H&E staining showed that there was no significant tissue necrosis or morphological changes in the OPDH-SV group compared with the control group (Fig. S15). These results confirm that OPDH-SV may be a promising safe and efficient anti-AS nano-prodrug treatment strategy.

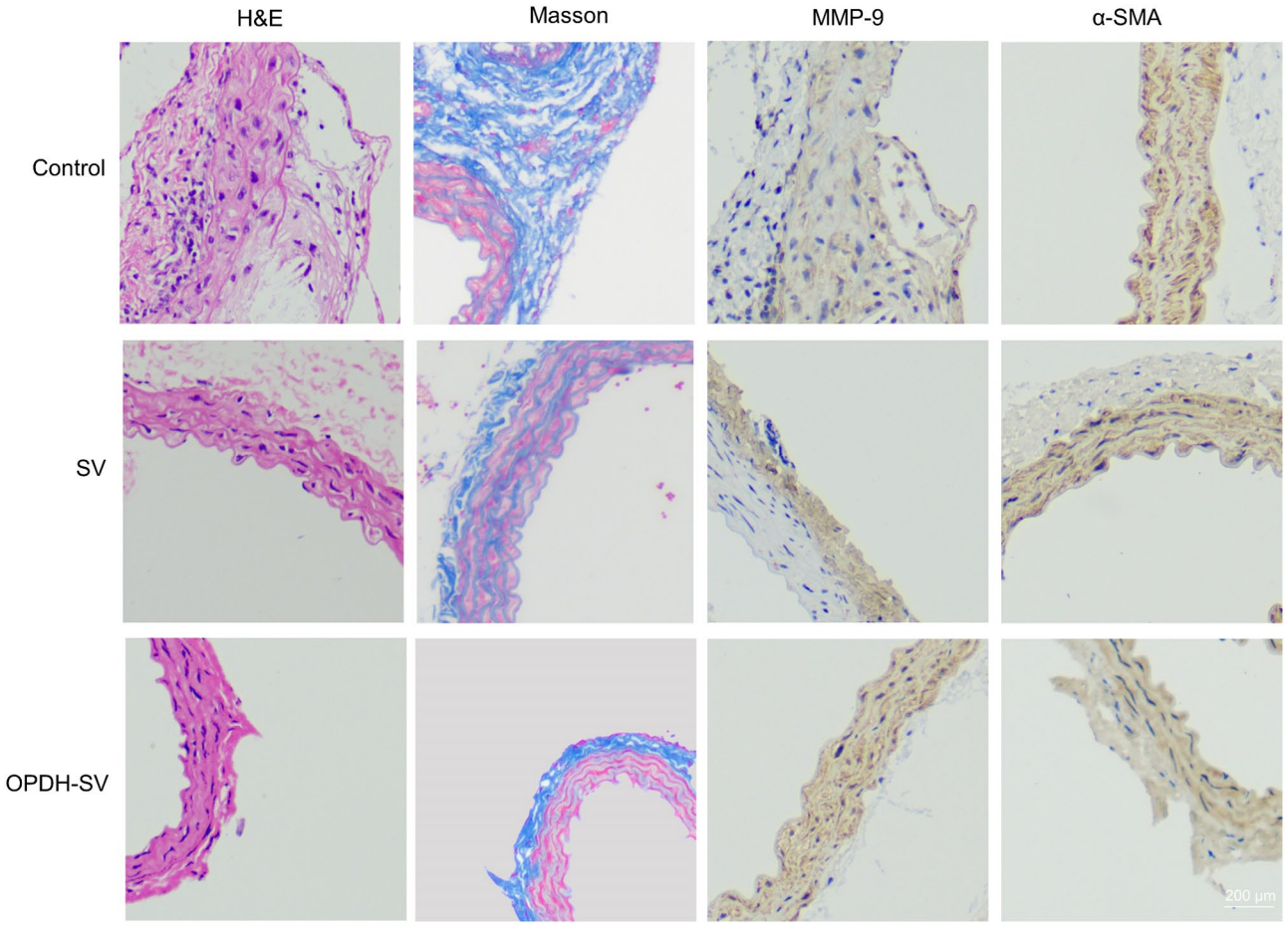

Fig. 6 Histological analysis of aortic arch sections from atherosclerotic mice after different drug treatments. Representative photographs of aortic arch sections stained with H&E staining, Masson staining, MMP-9 antibody staining, and α-SMA antibody staining, scale bar = 200 μm

Conclusion

In summary, we have successfully prepared a novel zwitterionic nano-prodrug OPDH-SV with active transcytosis, long-acting circulation in vivo, and plaque-targeting for atherosclerotic therapy. In the environment of high ROS concentration at the lesion site, it can trigger the breaking of the oxalate bond in OPDH-SV, thereby releasing simvastatin, which exerts its antioxidant, hypolipidemic and foam cell formation effects. In the ApoE$^{-/-}$ mouse model, OPDH-SV demonstrated significant therapeutic efficacy and good in vivo safety, while effectively reducing the cytotoxicity of the drug and achieving long-term circulation in vivo. More importantly, OPDH-SV can achieve high enrichment of atherosclerotic plaques through the "endocytosis-efflux" mechanism, which plays an excellent therapeutic role. Therefore, OPDH-SV is expected to be a potential excellent drug candidate in the field of atherosclerotic therapy.

Supplementary Information

The online version contains supplementary material available at https://doi.org/10.1186/s12951-025-03232-1.

Supplementary Material 1

Supplementary Material 2

Acknowledgements
Not applicable.

Author contributions
H. Y. conceived the experimental design, conducted the experiment, and wrote the paper. Y. L. and M.S. contributed to the design and revision of the manuscript and provided financial support. M. G., Q. G., L. Z., M. L. and H. L. contributed to the design of the experimental method and collated the data. G. Q. and Q.Y. supervised the conduct of the experiment. The final manuscript has been read and approved by all authors.

Funding
This work was supported by the National Natural Science Foundation of China (U24A20477), Jilin Province Natural Science Foundation (YDZJ202401490ZYTS), Science and Technology Research Project of the Education Department of Jilin Province (JJKH20241342KJ), Jilin University Bethune Medical Department (2023B16 and 2022JBGS04) and "Xinghai Project" of China-Japan Friendship Hospital of Jilin University (XHYF202304, XHQMX20232).

Data availability
No datasets were generated or analysed during the current study.

Declarations

Ethics approval and consent to participate
All animal experiments were performed under the guidance of the Animal Ethics and Experiment Committee of Jilin University. All animal experimental were approved by the Animal Ethics and Experiment Committee of Jilin University (approval number: 2024 extension No. 552).

Consent for publication
All the authors have approved the manuscript to publish.

Competing interests
The authors declare no competing interests.

Received: 11 December 2024 / Accepted: 11 February 2025
Published online: 06 March 2025

References

1. Psarros C, Lee R, Margaritis M, Antoniades C. Nanomedicine for the prevention, treatment and imaging of atherosclerosis. Nanomedicine-Nanotechnology Biology Med. 2012;8:59–68.
2. Yang X, Qin Q, Wang Y, Ma Z, Li Q, Zhang F, Han Y, Wang H. Knowledge, attitudes, and practices regarding cardiovascular disease prevention among middle school students in China: a cross-sectional study. Front Public Health. 2024;12:1301829.
3. Mingbo Liu X, He X, Yang Z, Wang. Key points of the Chinese Cardiovascular Health and Disease Report 2023. Chin J Cardiovasc. 2024;29:305–24.
4. Bonetti PO, Lerman LO, Napoli C, Lerman A. Statin effects beyond lipid lowering–are they clinically relevant? Eur Heart J. 2003;24:225–48.
5. Aronow WS. MRC/BHF Heart Protection Study of cholesterol lowering with simvastatin in 20,536 high-risk individuals: a randomized placebo-controlled trial. J Am Geriatr Soc. 2003;51:717–8.
6. Jain MK, Ridker PM. Anti-inflammatory effects of statins: clinical evidence and basic mechanisms. Nat Rev Drug Discovery. 2005;4:977–87.
7. Gurevich VS, Shovman O, Slutzky L, Meroni PL, Shoenfeld Y. Statins and autoimmune diseases. Autoimmun rev. 2005;4:123–9.
8. Hu B, Boakye-Yiadom KO, Yu W, Yuan ZW, Ho W, Xu X, Zhang XQ. Nanomedicine Approaches for Advanced Diagnosis and Treatment of Atherosclerosis and related ischemic diseases. Adv Healthc Mater. 2020;9:e2000336.
9. Gotto AM. Antioxidants, statins, and atherosclerosis. J Am Coll Cardiol. 2003;41:1205–10.
10. Gonzalez ER. Antiplatelet therapy in atherosclerotic cardiovascular disease. Clin Ther. 1998;20:18–41.
11. Blanco E, Shen H, Ferrari M. Principles of nanoparticle design for overcoming biological barriers to drug delivery. Nat Biotechnol. 2015;33:941–51.
12. Chan CKW, Zhang L, Cheng CK, Yang H, Huang Y, Tian XY, Choi CHJ. Recent advances in managing atherosclerosis via Nanomedicine. Small. 2018;14.
13. Blaha MJ, Abdelhamid M, Santilli F, Shi Z, Sibbing D. Advanced subclinical atherosclerosis: a novel category within the cardiovascular risk continuum with distinct treatment implications. Am J Prev Cardiol. 2023;13:100456.
14. Shah SR, Werlang CA, Kasper FK, Mikos AG. Novel applications of statins for bone regeneration. Natl Sci Rev. 2015;2:85–99.
15. Istvan ES, Deisenhofer J. Structural mechanism for statin inhibition of HMG-CoA reductase. Science. 2001;292:1160–4.
16. Rautio J, Meanwell NA, Di L, Hageman MJ. The expanding role of prodrugs in contemporary drug design and development. Nat Rev Drug Discov. 2018;17:559–87.
17. Xiang J, Liu X, Yuan G, Zhang R, Zhou Q, Xie T, Shen Y. Nanomedicine from amphiphilizedprodrugs: Concept and clinical translation. Adv Drug Deliv Rev. 2021;179:114027.
18. Deng Z, Hu J, Liu S. Reactive oxygen, Nitrogen, and Sulfur species (RONSS)-Responsive polymersomes for triggered drug release. Macromol Rapid Commun. 2017;38.
19. Broaders KE, Grandhe S, Fréchet JM. A biocompatible oxidation-triggered carrier polymer with potential in therapeutics. J Am Chem Soc. 2011;133:756–8.
20. Li C, Wallace S. Polymer-drug conjugates: recent development in clinical oncology. Adv Drug Deliv Rev. 2008;60:886–98.
21. Greco F, Vicent MJ. Combination therapy: opportunities and challenges for polymer-drug conjugates as anticancer nanomedicines. Adv Drug Deliv Rev. 2009;61:1203–13.
22. Schlenoff JB. Zwitteration: coating surfaces with zwitterionic functionality to reduce nonspecific adsorption. Langmuir. 2014;30:9625–36.
23. Jin Q, Chen Y, Wang Y, Ji J. Zwitterionic drug nanocarriers: a biomimetic strategy for drug delivery. Colloids Surf B Biointerfaces. 2014;124:80–6.
24. Zou H, Wang Z, Feng M. Nanocarriers with tunable surface properties to unblock bottlenecks in systemic drug and gene delivery. J Control Release. 2015;214:121–33.
25. Chen S, Zhong Y, Fan W, Xiang J, Wang G, Zhou Q, Wang J, Geng Y, Sun R, Zhang Z, et al. Enhanced tumour penetration and prolonged circulation in blood of polyzwitterion-drug conjugates with cell-membrane affinity. Nat Biomed Eng. 2021;5:1019–37.
26. Xiang J, Shen Y, Zhang Y, Liu X, Zhou Q, Zhou Z, Tang J, Shao S, Shen Y. Multipotent poly(tertiary Amine-Oxide) micelles for efficient Cancer Drug Delivery. Adv Sci (Weinh). 2022;9:e2200173.
27. Pandit S, Dutta D, Nie S. Active transcytosis and new opportunities for cancer nanomedicine. Nat Mater. 2020;19:478–80.
28. Liu Y, Huo Y, Yao L, Xu Y, Meng F, Li H, Sun K, Zhou G, Kohane DS, Tao K. Transcytosis of Nanomedicine for Tumor Penetration. Nano Letter. 2019;19:8010–20.
29. Zhou Q, Shao S, Wang J, Xu C, Xiang J, Piao Y, Zhou Z, Yu Q, Tang J, Liu X, et al. Enzyme-activatable polymer-drug conjugate augments tumour penetration and treatment efficacy. Nat Nanotechnol. 2019;14:799–809.
30. Zhao R, Ning X, Wang M, Wang H, Xing G, Wang L, Lu C, Yu A, Wang Y. A ROS-Responsive simvastatin Nano-Prodrug and its fibronectin-targeted Co-delivery System for Atherosclerosis Treatment. ACS Appl Mater Interfaces. 2022;14:25080–92.
31. Jiang S, Cao Z. Ultralow-fouling, functionalizable, and hydrolyzable zwitterionic materials and their derivatives for biological applications. Adv Mater. 2010;22:920–32.
32. Moore KJ, Sheedy FJ, Fisher EA. Macrophages in atherosclerosis: a dynamic balance. Nat Rev Immunol. 2013;13:709–21.
33. Wang Y, Li L, Zhao W, Dou Y, An H, Tao H, Xu X, Jia Y, Lu S, Zhang J, Hu H. Targeted therapy of atherosclerosis by a broad-spectrum reactive oxygen species scavenging nanoparticle with intrinsic anti-inflammatory activity. ACS Nano. 2018;12:8943–60.
34. Xu H, She P, Zhao Z, Ma B, Li G, Wang Y. Duplex responsive nanoplatform with Cascade Targeting for Atherosclerosis Photoacoustic diagnosis and multichannel combination therapy. Adv Mater. 2023;35:e2300439.
35. Cossarizza A, Baccarani-Contri M, Kalashnikova G, Franceschi C. A new method for the cytofluorimetric analysis of mitochondrial membrane potential using the J-aggregate forming lipophilic cation 5,5',6,6'-tetrachloro-1,1',3,3'-tetraethylbenzimidazolcarbocyanine iodide (JC-1). Biochem Biophys Res Commun. 1993;197:40–5.
36. Wang S, Zhang J, Li W, Chen D, Tu J, Sun C, Du Y. Hyaluronic acid-guided assembly of ceria nanozymes as plaque-targeting ROS scavengers for antiatherosclerotic therapy. Carbohydr Polym. 2022;296:119940.
37. Borén J, Chapman MJ, Krauss RM, Packard CJ, Bentzon JF, Binder CJ, Daemen MJ, Demer LL, Hegele RA, Nicholls SJ, et al. Low-density lipoproteins cause atherosclerotic cardiovascular disease: pathophysiological, genetic, and therapeutic insights: a consensus statement from the European Atherosclerosis Society Consensus Panel. Eur Heart J. 2020;41:2313–30.
38. Xu H, She P, Ma B, Zhao Z, Li G, Wang Y. ROS responsive nanoparticles loaded with lipid-specific AIEgen for atherosclerosis-targeted diagnosis and bifunctional therapy. Biomaterials. 2022;288:121734.
39. Zhao Z, Feng Y, Xiang J, Liu J, Piao Y, Shao S, Tang J, Zhou Z, Shen Y. Screening of Zwitterionic liposomes with Red Blood Cell-Hitchhiking and Tumor cell-active transporting capability for efficient Tumor Entrance. Adv Funct Mater. 2023;33.
40. Yuan G, Zhang Y, Shao S, Zhou Z, Tang J, Xiang J, Shen Y. Tumor permeable self-delivery nanodrug targeting mitochondria for enhanced chemotherapy. J Control Release. 2023;361:792–802.

Publisher's note